Journal of Microelectronics and Electronic Packaging (2017) **14**, 32-38

ISSN: 1551-4897

Addressing Flux Dip Challenges for 3-D Integrated Large Die, Ultrafine Pitch Interconnect

C. Marsan-Loyer,[1,*] D. Danovitch,[1] and N. Boyer[2]

***Abstract*—The requirement for closely coupled, highly integrated circuits in the semiconductor industry has spawned alternative packaging innovations such as 2.5-D/3-D integration. The incredible potential of this alternative comes with great challenges, not the least of which is the unprecedented reduction in package interconnection pitch. Market acceptance of new fine-pitch microelectronic products is strongly dependent on the development of flawless assembly processes that align with the traditional Moore-like expectation of higher performance without cost penalty. One such process is the application of flux to the interconnect surfaces to achieve effective joining. Insufficient flux quantity or flux activity can impede the formation of solid, reliable joints, whereas excessive quantities or activity can cause solder bridging or difficulties with downstream operations such as residue cleaning or underfill reinforcement. This delicate balance, already complex for traditional chip joining, is further challenged by the geometrical and spatial reductions imposed by pitch miniaturization, especially where large die, with over 100,000 interconnects, are concerned. This article presents an overall development protocol to evolving a flux dipping operation to production-level thermocompression assembly of large die (8 × 11 × 0.780 mm) with 11,343 ultrafine pitch (62 μm) copper pillar interconnections. After reviewing the state of the art for fluxing technology and detailing the specific technical issues, we present and defend the chosen flux application approach with its corresponding parameters of interest. Physical and chemical characterization results for selected flux material candidates are reported in conjunction with an analysis of how their properties correlate to the flux dip application parameters. As part of this fundamental understanding, we investigate and report on flux dip coating behavior and how it compares to other industrial dip coating applications. Finally, the results of process assembly experiments in a production-type environment are reviewed and discussed with respect to the previous characterizations. These experiments span downstream assembly process compatibility (i.e., cleaning and underfill) as well as product reliability.**

***Keywords*—3-D integration, dipping, flux, thermocompression bonding, ultrafine pitch**

The manuscript was received on November 22, 2016; revision received on January 11, 2017; accepted on January 29, 2017

The original version of this paper was presented at 49th International Symposium on Microelectronics (IMAPS'2016), October 11-13, 2016, Pasadena, CA.

[1]Université de Sherbrooke, 2500 boul. de l'Université, Sherbrooke, Québec, Canada

[2]IBM Canada, 23 boul, de l'Aéroport Bromont, Québec, Canada

*Corresponding author; email: catherine.marsan-loyer@c2mi.ca

Introduction

The past 5-10 years have seen flip chip interconnection densities scale at an unprecedented rate, driven largely by the potential to increase system performance using 2.5-D and 3-D configurations of through-silicon-via technology. Efforts to address the ensuing reductions in interconnect geometry and spacing have revealed shortcomings in the incumbent structures and processes that comprise the proven controlled chip collapse connection (C4) approach to flip chip assembly. An important example of innovation in this area is the use of copper pillar structures to reduce collapse during reflow, thereby averting solder bridging and mitigating underfill gap reduction [1]. Closely tied to this innovation is the shift to thermocompression bonding (TCB) for achieving the interconnection. Despite suffering a throughput disadvantage compared with the massively parallel furnace reflow approach, TCB has garnered significant acceptance for finer pitch (below 100 μm) applications. This is largely explained by the ability of TCB, through its force component, to compensate for the lack of collapse in Cu pillars as well as for the increased warpage inherent to the thinner Si interposers and organic substrates that are prevalent in finer pitch applications [2].

Shifting to such a new structure and process is not a trivial matter and requires painstaking attention to the individual aspects of the solder joint formation process. One such aspect is the preparation of the connection surfaces, specifically the removal of any oxides on the chip bumps or substrate receiving pad surfaces that may impede the formation of a metallurgically sound interconnection. While several techniques have been proposed, such as the use of formic acid or hydrogen atmospheres, the application of a flux material is still the prevalent choice, as it does not require any additional preparation of the chips nor special installations for hazardous chemicals [3-5]. Nonetheless, the challenges of finer pitches have encouraged the replacement of chip site flux spray techniques with a flux dipping approach that places the material only where needed, reducing the risks for flux bridging and residue after cleaning. Here, the die is lowered, with bumps or pillars facing down, into a flux film of predetermined depth, optimally about half of the height of the pillars or bumps [6]. Success of this selective means for flux application depends critically on the ability to precisely control and repeat the quantity of flux picked up. Too much flux can promote bridging while an insufficient amount can result in poorly joined or completely open connections.

doi:10.4071/imaps.348081

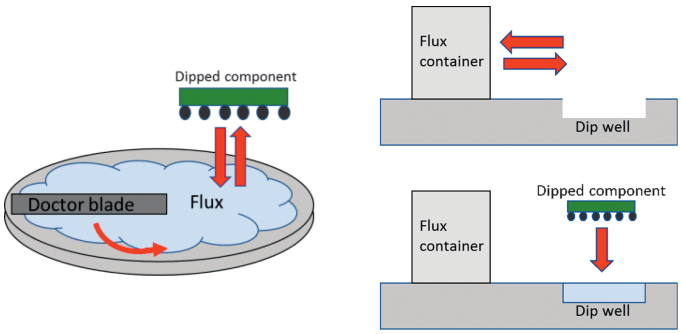

(a) Rotary dip plate **(b)** Linear dip well plate with container

Fig. 1. Dip fluxing techniques usually used.

There are two generally accepted flux dipping techniques. The rotary plate approach (Fig. 1a) uses a blade to control flux film thickness and thereby flux dip depth [6]. While very useful for prototyping due to its versatility for adjusting dip depth, constant exposure of the flux to air risks significant variation in flux performance due to continual evaporation of any volatile components. On the other hand, the linear dip well plate approach (Fig. 1b) preserves the majority of flux material in a sealed reservoir, rendering this method more conducive to large-scale production of volatile fluxes, though careful monitoring of the reservoir to dip well flux transfer effectiveness is necessary [7].

Naturally, the flux material and its dipping process must also be compatible with assembly process steps downstream from chip joining. Finer pitches render flux residue cleaning techniques more difficult, to the point that a number of low-residue, no-clean fluxes have been proposed [8,9]. Similarly, the capillary underfill process, still favored for very large die sizes, becomes increasingly susceptible to flux residues at the smaller gaps of fine pitch configurations that induce inconsistent flow fronts and resultant voiding as well as regions for potential delamination.

This article presents a methodology to characterize and understand the behavior and reactions of a flux for fine pitch dipping. The methodology is validated in the course of a dip flux selection process and compared with the practical behavior in a production-level flip chip assembly environment comprising TCB and capillary underfill.

Theory of Flux Dipping Behavior

Flux materials are typically complex in their chemical nature, usually composed of an organic acid for deoxidation, an alcohol component (e.g., isopropyl acid or carboxylic acid) to reduce surface tension and ease wetting, and other agents that control its flow properties and chip tacking capability. As such, predicting and understanding its process behavior requires both chemical analyses and rheological characterization. The latter can be modeled for a dipping process by applying the principles of coating with a viscous fluid, which is best described by the Landau-Levich-Dejarguin (LLD) law with corrections applied by Tallmadge and White for coated fluid thicknesses approaching the diameter of the solid to be coated, as is the case with fine pitch pillar dipping [10,11]. Equation (1) defines this relationship:

$$h = \frac{1.34rCa^{2/3}}{1 - 1.34Ca^{2/3}} \tag{1}$$

$$Ca = \frac{\mu \times v}{\sigma} \tag{2}$$

where h is the thickness of the withdrawn fluid, r is the radius of the spherical or cylindrical object that is dipped, and Ca is the capillary number, the latter being defined in equation (2) as a function of viscosity μ, surface tension σ, and withdrawal speed v. This can be further refined by the Weber number to account for inertial effects [9]:

$$We = \frac{\rho v^2 r}{\sigma} \tag{3}$$

$$h = \frac{rCa^{2/3}}{1 - We} \tag{4}$$

where ρ is the fluid density. Finally, equation (5) adds to h the additional "drag" thickness δ of viscous fluids withdrawn at low speed, where L is the dip depth.

$$\delta = \sqrt{\frac{\mu L}{\rho v}} \tag{5}$$

It becomes evident from these equations that viscosity is an important parameter in the characterization of a fluid to be dipped. In fact, by understanding and analyzing the means by which viscosity is calculated using a plate rheometer, namely by assessing the fluid's storage modulus G', loss modulus G'', and angular frequency ω, a thorough knowledge of the fluid's viscoelastic behavior can be acquired. The relationships between viscosity and these variables are shown in equations (6) and (7):

$$G = \sqrt{(G')^2 + (G'')^2} \tag{6}$$

$$\mu = G/\omega \tag{7}$$

A number of characteristics can be derived by comparing the G' and G'' curves. For example, a situation where $G' > G''$ suggests a solid-like behavior, whereas the opposite implies a more liquid-like activity. Further, the plateau value before $G' = G''$ can be used to evaluate the internal cohesion properties [12,13].

Experimental Method

A. Laboratory Characterization

Three different commercial flux candidates were chosen for this evaluation. Two were water soluble with significantly different stated viscosities, whereas the third was a no-clean flux. The three candidates were thoroughly characterized by

analytical laboratory tests. Those pertinent to discussion in this article are viscosity, surface tension, and Fourier transform infrared spectroscopy (FTIR). The tests were respectively performed on a torque-type plate rheometer with a Noüy ring and a Nicolet FTIR. All tests were conducted with a minimum of three replicates.

B. Physical Characterization and Dimensional Analysis

Because the aforementioned LLD laws are very sensitive to the fluid's speed regimen and evaporation, a dimensional analysis approach following the Buckingham theorem was used [14]. Equation (8) shows the relationship that is obtained when considering the material's withdrawn mass m, its withdrawal speed v, its viscosity μ, and the dipped object diameter d for the determination of a dimensionless constant Lo:

$$Lo = \frac{mv}{\mu d^2} \tag{8}$$

The analysis was conducted by establishing a sphere dipping test setup, inspired by the physical observation approach adopted by Wei, and allowing for variation of withdrawal speed and dip depth [7]. The setup could accommodate different sphere diameters in both individual sphere form and chip/substrate form. The tests were conducted on an Instron tool (Series IX, model 43K2), on which the speed was fixed. The spheres were vacuum held on the dipping head and then dipped on a dipping plate of known depth, which was calculated to be half the diameter of the spheres, for a dwell time of 1 s after the sphere made contact with the bottom of the dip plate. In this manner, spheres were subjected to dipping experiments. Masses were measured before and after the dipping process after which values for Lo were calculated.

C. Assembly Evaluations

Parts used for assembly comprised a preassembled Si interposer on a laminate and an 8 × 11× 0.780 mm top die to complete the 3-D assembly. Interconnections were SAC solder–coated Cu pillars at 62-μm minimum pitch placed on Ni/Au pads. Chip joining was achieved by TCB. The flux dipping was performed on the same tool varying the withdrawal speed between 0.5 and 8.3 mm/s. The bonding profile comprised a 5-s ramp up to the bonding temperature (400°C) for a soak time of 20 s with a pressure of 0.5 N, all processes on a heated stage (150°C). The subsequent cleaning, where required, used deionized water in automated spray tooling. Underfilling was by capillary means using a qualified IBM underfill.

The performance of the fluxes in the assemblies was evaluated by destructive chip pull inspections and cross sections. The chip pull test was performed by attaching a pull stud to the top chip with glue. The top chip was then vertically separated from the interposer with an Instron tool (Series 8800, model 8874), enabling tensile force data acquisition and visual inspection. After selection of a preferred flux candidate and its optimal process parameters, a number of parts were processed through the full commercial assembly flow using both the preferred flux and a previously qualified control flux. Final assemblies were subjected to deep thermal cycling (DTC) and highly accelerated stress test (HAST), with appropriate electrical and acoustic microscopy assessments. Both tests included a Jedec Level 3 preconditioning step that simulates parts shipping and card attach: thermal shock, bake, humid environment, and bake. Specific conditions of each test are described in Table IV of the Results section.

Results and Discussion

A. Analytical Laboratory Characterization

The laboratory characterization of the fluxes provided useful insight into their expected behaviors before any dipping or assembly experimentation. FTIR analysis revealed that, while all fluxes exhibited the presence of the –OH group, their relative peak locations and amplitudes allowed interpretation of relative volatility and resultant susceptibility to aging. As presented in Table I, Flux 2 has a high concentration of alcohol, more precisely isopropyl alcohol, making it more vulnerable to such flux aging.

On the other hand, Fluxes 1 and 3 have the same –OH group but at a lower intensity peak, indicating a lesser concentration [15]. Thus, being less volatile than pure alcohol, Fluxes 1 and 3 are expected to be more stable during prolonged exposure to air. This information suggests the use of the linear dip well plate method for Flux 2 to minimize evaporation and maintain consistent behavior. Beyond the absolute viscosity values shown in Table I, interpretation of rheometer data showed additional predictive behavior. A constant viscosity under varied stress for Flux 2 is indicative of Newtonian behavior (Fig. 2b), which was not the case for Fluxes 1 and 3. Further analysis of the storage and loss modulus (G' and G'') curves revealed liquid-only viscoelastic behavior, suggesting favorable conditions for consistent wetting. Flux 1 behaved initially like a solid but changed to a liquid behavior under a 0.002 Pa stress and exhibited a relatively high G''/G' of 0.82 (Fig. 2a). This high ratio indicates that the flux does not have a good internal structure elasticity and would not retain its

Table I
Analytical Laboratory Characterization Results

	Flux 1	Flux 2	Flux 3
Flux type	Water soluble	Water soluble	No-clean
Viscosity (cP)	200 k	8 k	600 k
Surface tension (N/m)	0.698	0.0445	Unmeasurable with Noüy ring
FTIR	Presence of –OH	Presence of high concentration –OH	Presence of –OH

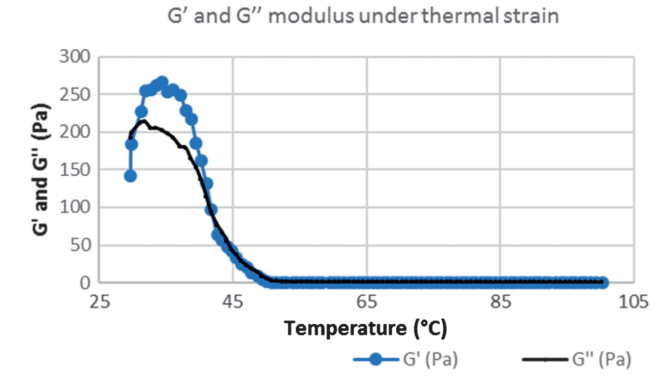

(a) G′ and G″ graph for Flux 1

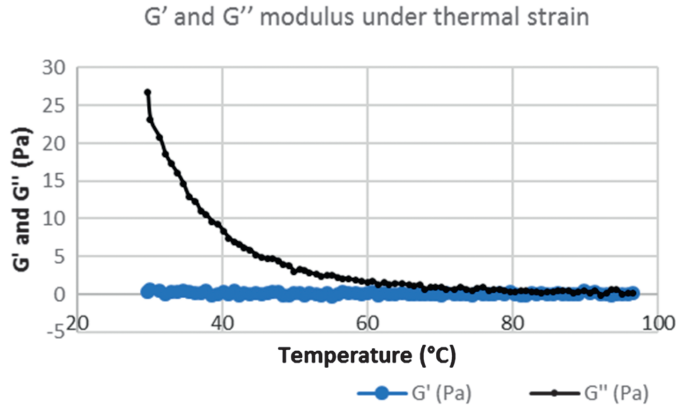

(b) G′ and G″ graph for Flux 2

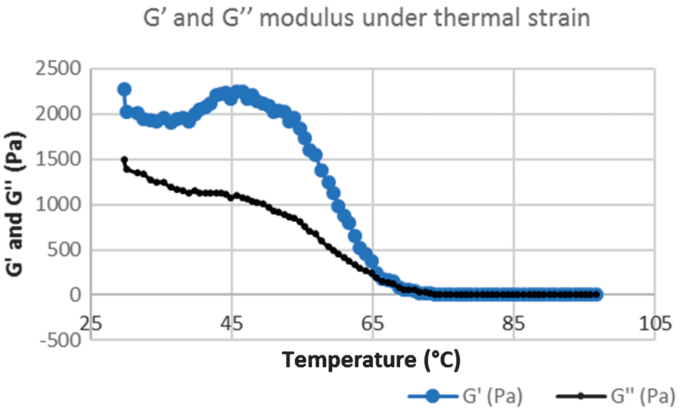

(c) G' and G'' graph for Flux 3

Fig. 2. G' and G'' graph for Fluxes 1, 2, and 3 tested under thermal strain.

form for long without flowing [12,13]. The surface tension measurements (Table I) appear to be in sync with this analysis, where the better flow propensity of Flux 2 leads to superior wetting and coating as compared with Flux 1. On the other hand, these results suggest potential climbing risks for Flux 1, recommending limited dip residence times. Flux 3, while also exhibiting an initial solid behavior, showed a lower G''/G' ratio of 0.39, suggesting better internal elasticity with less tendency to flow (Fig. 2c). During the TCB process, the fluxes are also subjected to heat from the dipping head, which was preheated (150°C) to reduce process time. Both heated and nonheated dip heads have been tested with minimal process impact observed.

Table II
Modeling of Flux 2 Mass for Different Sphere Diameters Using LLD Corrected Laws

Sphere diameter (m)	Calculated mass (by corrected LLD and drag thickness additions [μg])	Measured mass (μg)
29E-06	0.335	0.413
3.15E-03	4.12E + 04	5.00E + 03
4.75E-03	6.21E + 04	1.10E + 04
9.5E-03	7.49E + 05	1.22E + 05

B. Physical Characterization of Dipping

Flux 2, as shown by laboratory characterization above, is a Newtonian fluid and can therefore be modeled using the corrected LLD laws (including drag) and the dimensional analysis techniques. Despite its high viscosity and tendency to evaporate, and despite withdrawal speeds approaching the limit of the capillary regimen, the LLD corrected laws approximated fairly well the measured values of withdrawn flux mass, as shown in Table II.

The dimensional analysis using the relationship of equation (7) provided an even more accurate prediction (Table III). *Lo* was calculated at withdrawal speeds of 0.5, 2, and 8.3 mm/s for various macroscopic sphere sizes then used to predict the withdrawn mass of flux on Cu μpillars. Actual mass was then measured at a die level with 11,343 pillars to minimize error contributions of the measurement tool. These results suggest that flux parameters can be initially established using macroscopic spheres without the need of actual hardware and painstaking measurements.Accuracy of these predictions could be further improved by addressing the principal sources of error, namely the uncertainty caused by the weight scale (±100 μg) that was not precise enough to measure individual 29-μm diameter spheres, flux alcohol evaporation, and withdrawal speed precision.

Such mass modeling was not possible for the non-Newtonian Fluxes 1 and 3 in that viscosity variation with strain could not be measured with the current rheometer. Nevertheless, measurements of mass demonstrated that all three fluxes exhibit the same phenomenon of increased mass pickup as a function of increased withdrawal speed. This can be easily observed (Fig. 3) with Flux 1.

Table III
Modeling of Flux 2 Mass on Cu μpillars for Different Withdrawal Speeds Using Dimensional Analysis

Withdrawal speed (mm/s)	Predicted weight (μg)	Actual measured weight (μg)
0.5	0.660	0.420
2	0.468	0.413
8.33	0.271	0.166

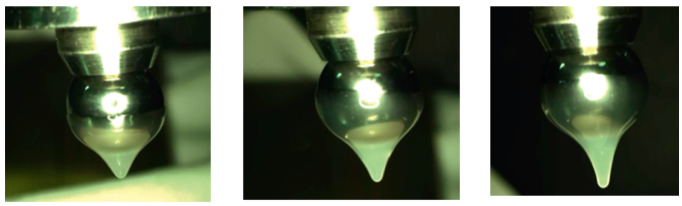

Fig. 3. Flux 1 mass as a function of withdrawal speed.

C. Assembly Evaluations

The results of the laboratory and physical analyses provided a first-order approximation of dipping variables to be used in assembly experiments for the three flux candidates. Using the chip pull destructive analyses to assess wetting and cleanliness responses, a series of matrices progressively reduced the number of candidates and fine-tuned the dipping parameters, specifically dip depth, flux residence time, and withdrawal speed. For example, Fig. 4 shows the number of nonwetted Cu pillars as a function of withdrawal speed for the three fluxes. We can then conclude that the withdrawal speed can be adjusted to maximize wetted interconnections. Nonetheless, it should be recognized that withdrawal speed is but one important parameter to achieve a high yield of perfect parts. For example, the TCB process parameters can play a very important role, but in this research, they were only optimized to the point of obtaining satisfactory bonding and enabling relative comparison of the studied fluxes. The overall results of these matrices led to the selection of Flux 2 and a corresponding set of optimized dip parameters that demonstrated defect-free wetting, which was demonstrating that some fluxes formulation are in fact, better adapted to the dipping process.

From a cleanliness perspective, both Fluxes 1 and 2 initially left some degree of undesirable residues which were shown by subsequent scanning electron microscopy (SEM) analysis to be metallic (Sn) in nature for Flux 1 and organometallic (organo-tin) in nature for Flux 2. The cleaning processes were modified to account for these residues with adjustments being most effective for Flux 2 (Fig. 5), which was confirmed with a clean, no-void, part with acoustic microscopy (Fig. 6). On the other hand, Flux 3 was found to leave a significant amount of residue (Fig. 7), which was somewhat surprising given its designation as a no-clean flux. It was hypothesized

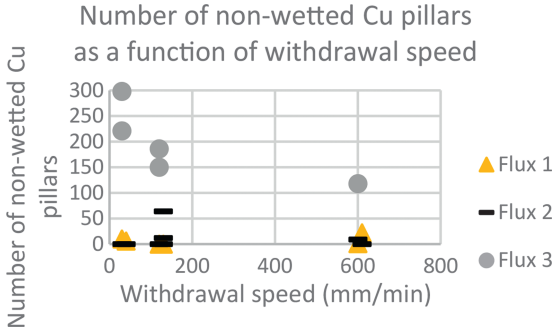

Fig. 4. Number of nonwetted Cu pillars (of 11,343 total) as a function of withdrawal speed.

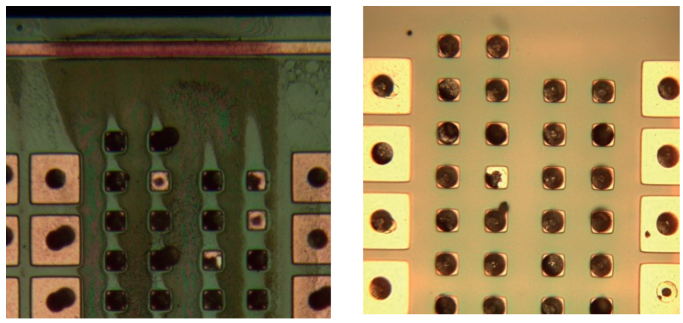

Fig. 5. Impact of cleaning adjustments on degree of residue for Flux 2 as tested (smallest pitch of 62 μm).

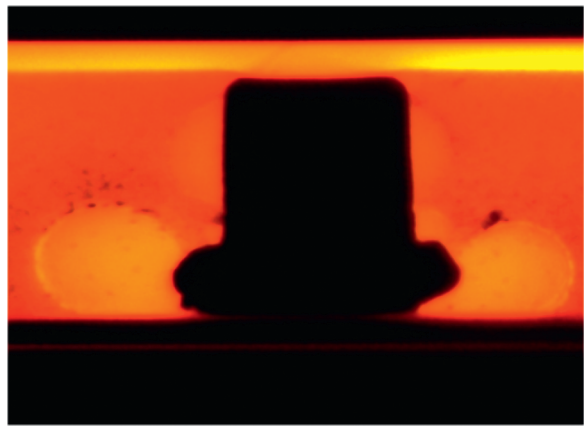

Fig. 6. Void-free assembly for Flux 2 (top chip of 8 × 11 mm) result by acoustic microscopy.

and validated that the degree of residue was strongly related to the short temperature profile inherent to TCB.

The overall findings of the aforementioned matrices recommended the selection of Flux 2 for an integrity/reliability evaluation build. As part of this evaluation, construction

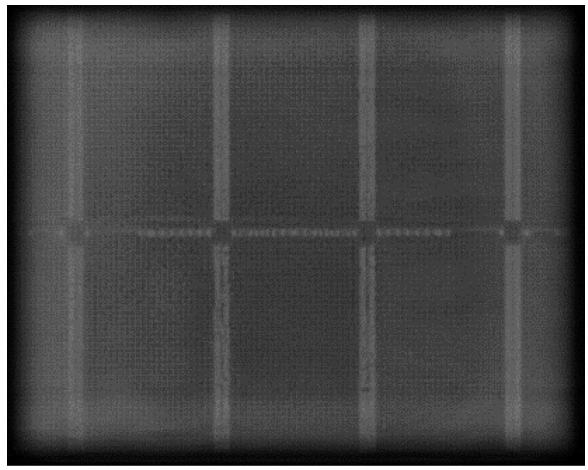

Fig. 7. Flux 3 residue ~20-μm diameter Cu pillar in cross section under UV light as inspected.

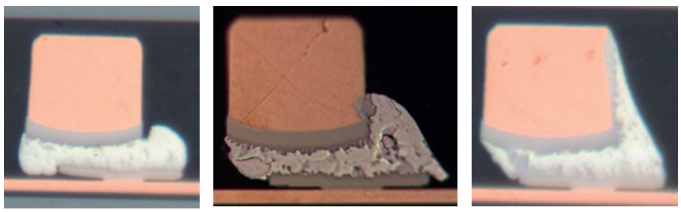

Fig. 8. Flux 2 solder climb variation across 11 mm length of chip as inspected on 20-µm diameter Cu pillar.

analysis demonstrated that, while nominal dip depth was a little over half the height of the Cu µpillar, process deviations in chip versus dip well planarity could lead to some degree of variability in dip depth that would in turn alter the structure of the interconnections. This is shown in Fig. 8 where different degrees of solder climb and intermetallic formation across the length of the chip are indicative of varying dip depths.

Reliability stress testing was performed as summarized in Table IV, including comparisons to a previously qualified flux. No electrical fails were found, confirming the selection of Flux 2 as a suitable dip flux candidate and suggesting that the aforementioned degree of dip depth variation and its resultant impact on interconnect structure could be tolerated in a normal production environment. In that 78 parts were tested, divided between the previously qualified flux and the Flux 2, this represents promising positive reliability feedback but recommends further qualification of Flux 2 with a larger population of assemblies.

A small number of parts exhibited minor visual anomalies after Jedec level 3 preconditioning. However, subsequent x-sectional analysis (Fig. 9) related the anomalies to incoming defects and showed that no flux residues were evident and that the Cu pillars in the zone of interest did not exhibit any signs of questionable integrity.

Table IV
Summary of Reliability Assessment

Reliability test	Detail	Pass
HAST	110°C/85% RH/264 h/3.7 V	Yes
DTC	−40/125°C/1,000 cycles	Yes

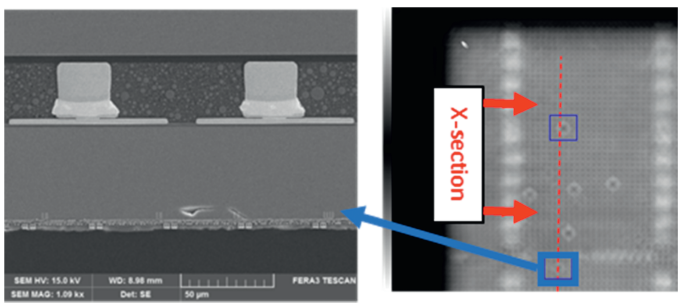

Fig. 9. DTC defect cross section inspection (left) based on C-mode scanning acoustic microscope observations (right).

Conclusions

A systematic approach was developed for the selection, characterization, screening, and evaluation of fluxes for fine pitch flux dipping in a thermocompression chip join environment. The approach was validated for three commercial fluxes of interest, demonstrating a clear relationship between fundamental laboratory analysis, physical characterization, and process behavior.

FTIR analysis showed the presence of alcohol in all three fluxes tested, but in different concentrations and types, providing important recommendations for preventing flux aging during production-scale manufacturing. Rheological analysis was also proven to be of significant value for predicting flux behavior, allowing the assessment of Newtonian type, propensity to flow, liquid-solid transition behavior, and wetting tendency.

The laboratory analysis was complemented by a macroscopic sphere dipping protocol that enabled dip modeling on the Newtonian Flux 2. Both the LLD corrected laws for dip coating and a dimensional analysis approach approximated fairly well the expected dipping results at the microscopic level of fine pitch Cu pillars, suggesting that this macroscopic dipping protocol could be used as a quick yet accurate initial assessment of flux performance without consuming valuable hardware.

Subsequent assembly testing of the fluxes demonstrated correlated behavior to the aforementioned characterizations and used wetting and cleanliness responses to ultimately recommend a specific flux candidate for reliability testing. The chosen candidate proved its viability through a full assembly build and subsequent DTC and HAST stress testing.

As for future work, a larger sample of parts would be necessary to fully validate the use of the chosen flux with the associated dipping parameters. As part of this effort, the TCB process should also be carefully adapted. Finally, because no-clean flux is a preferred option in industrial manufacturing, additional no-clean flux studies are recommended, be it a revised version of Flux 3 used in this research or a completely new flux.

Acknowledgments

The authors would like to thank Pierre Beaulieu and François Racicot at IBM's analytical labs for their expertise and assistance and François Arguin for his precious help on the assembly line. They would also like to recognize the important contribution of the MiQro Innovation Collaboration Center (C2MI) for access to its resources and laboratories. This work was supported by NSERC Canada and Prompt Quebec as part of an NSERC-IBM Canada Industrial Research Chair in Smarter Microelectronics Packaging for Performance Scaling.

References

[1] B.K. Appelt, H. Chung, C. Chienfan, and R. Wang, "Fine pitch flip chip chip scale packaging," Proceedings of the 18th European Microelectronics and Packaging Conference (EMPC), Brighton, United Kingdom, pp. 1-4, 2011.

[2] S.W. Yoon, D.W. Yang, J.H. Koo, M. Padmanathan, and F. Carson, "3D TSV processes and its assembly/packaging technology," IEEE International Conference on 3D System Integration, Boston, MA, 2009.

[3] B. Schmaltz, "Packaging materials for 2.5/3D technology," Proceedings of the 15th International Symposium and Exhibition on Advanced Packaging Materials (APM 2013), Vol. 2, No. 8, pp. 93-101, 2013.
[4] T.K. Lee, S. Zhang, C.C. Wong, and A.C. Tan, "Assessment of fluxless solid liquid interdiffusion bonding by compressive force of Au-PbSn and Au-SAC for flip chip packaging," *IEEE Transactions on Advanced Packaging*, Vol. 32, No. 1, pp. 116-122, 2009.
[5] H. Matsuki, H. Matsui, E. Watanabe, and F.D. Div, "Fluxless bump reflow using carboxylic acid," International Symposium on Advanced Packaging Materials, Baltimore, Maryland, pp. 135-139, 2001.
[6] E. Klaver and S.P. Manager, "Controlled package on package placement," [Online]. http://www.assembleon.com/images/User data/Downloads/Whitepapers/Package-on-Package.pdf, 2014. Accessed January 1, 2014.
[7] Z. Wei, J. Li, and H. Lei, "Study of a dipping method for flip-chip flux coating," *Microelectronics and Reliability*, Vol. 54, No. 11, pp. 2479-2486, 2014.
[8] A. Mackie, "Solder paste and flux dip depth: II," Indium. [Online]. http://blogs.indium.com/blog/smt-solder-paste/page/2, 2011.
[9] R.N. Master, A. Dubey, M. Guardado, O.T. Ong, B. Donges, and F. Okada, "Novel jet fluxing application for advanced flip chip and BGA/CGA packages," Proceedings of the 50th Electronic Components and Technology Conference (Cat. no.00CH37070), Las Vegas, Nevada, pp. 1185-1188, 2000.
[10] D. Quéré, "Fluid coating on a fiber," *Annual Review of Fluid Mechanics*, Vol. 31, No. 1, pp. 347-384, 1999.
[11] O. Bin Yusuf, "Improved non-linear solution of dip coating flow," MS thesis, The University of Western Ontario, London, Ontario, Canada, 2012.
[12] R. Durairaj, S. Mallik, A. Seman, A. Marks, and N.N. Ekere, "Viscoelastic properties of solder pastes and isotropic conductive adhesives used for flip-chip assembly," Proceedings of the 33rd IEEE/CPMT International Electronic Manufacturing Technology Symposium, Penang, Malaysia, pp. 1-8, 2008.
[13] R. Durairaj, S. Mallik, A. Seman, A. Marks, and N.N. Ekere, "Rheological characterization of solder pastes and isotropic conductive adhesives used for flip-chip assembly," *Journal of Materials Processing Technology*, Vol. 209, No. 8, pp. 3923-3930, 2009.
[14] D. Huilier, "Analyse dimensionnelle et similitude," Chapitre 6 *Notes cours Polytech.*, No. 1, pp. 1-5, 2014.
[15] D. Gennet, *Introduction à la Spectroscopie Infrarouge (I.R.)*, Laboratoire de Synthese Organique Ecole Polytechnique, 2004.